Soliton and kink jams in traffic flow with open boundaries

Masakuni Muramatsu and Takashi Nagatani
Division of Thermal Science, College of Engineering, Shizuoka University, Hamamatsu 432-8561, Japan
(Received 3 November 1998)

Soliton density wave is investigated numerically and analytically in the optimal velocity model (a car-following model) of a one-dimensional traffic flow with open boundaries. Soliton density wave is distinguished from the kink density wave. It is shown that the soliton density wave appears only at the threshold of occurrence of traffic jams. The Korteweg–de Vries (KdV) equation is derived from the optimal velocity model by the use of the nonlinear analysis. It is found that the traffic soliton appears only near the neutral stability line. The soliton solution is analytically obtained from the perturbed KdV equation. It is shown that the soliton solution obtained from the nonlinear analysis is consistent with that of the numerical simulation.
[S1063-651X(99)04807-2]

PACS number(s): 05.40.−a, 47.55.−t, 89.40.+k

I. INTRODUCTION

Recently, traffic problems have attracted considerable attention [1–30]. Uniform traffic flow is stable at low density. When the car density is higher than the critical density, the uniform traffic can be unstable, with localized regions of high density and low velocity spontaneously appearing. These density waves preserve their shape and move backward with constant speed; they correspond to the ''phantom'' traffic jams, which appear on a highway for no apparent reason.

Kerner and Konhauser have found the single-pulse density wave in numerical simulations of the hydrodynamic traffic model [22]. The profile of the single-pulse density wave is shown in Fig. 1(b). They have applied the linear stability analysis to the traffic model but it has not been analyzed by the nonlinear analysis method. Lately, Kurtze and Hong have derived the Korteweg-de Vries (KdV) equation from the hydrodynamic model by the use of the nonlinear analysis method. They have concluded that the single-pulse density wave is the soliton [26]. The soliton solution of the density wave has the shape shown in Fig. 1(c). However, the soliton solution in Fig. 1(c) is not consistent with the single-pulse density wave in Fig. 1(b). It is conjectured that the single-pulse density wave found by Kerner and Konhauser is not ''soliton'' but is similar to the asymmetric kink-antikink density wave. On the other hand, Komatsu and Sasa have derived the modified KdV equation from the car-following model [27]. They have showed that the density wave has the kink-antikink shape shown in Fig. 1(a). By comparing the analytical solution with the simulation result, they have confirmed that the phantom traffic jam is the symmetric kink-antikink density wave.

The above observations have brought to our attention the need for distinguishing between the soliton density wave and the kink-antikink density wave. We describe briefly the soliton and kink soltions in terms of the nonlinear wave equations. The soliton is a solution of the KdV equation:

$$\frac{\partial R}{\partial T}-\frac{\partial^3 R}{\partial X^3}+R\frac{\partial R}{\partial X}=0, \tag{1}$$

where X and T are space and time variables. Its solution is described by

$$R(X,T)=A\,\mathrm{sech}^2\left\{\sqrt{(A/12)}\left(X-\frac{AT}{3}\right)\right\}, \tag{2}$$

where A is the amplitude.
On the other hand, the kink is a solution of the modified KdV equation:

$$\frac{\partial R}{\partial T}-\frac{\partial^3 R}{\partial X^3}+\frac{\partial R^3}{\partial X}=0. \tag{3}$$

Its solution is described by

$$R(X,T)=A\tanh\{\sqrt{(1/2)}A(X-A^2T)\}. \tag{4}$$

Thus, the kink solution is definitely different from the soliton solution. The kink soliton has the plateau within the density wave shown in Fig. 1(a). The propagation velocity of the kink is definitely different from that of the soliton.

Until now, the soliton density wave predicted by Kurtze and Hong is not observed in the traffic simulations. There is an important question whether or not the soliton density wave appears in the traffic simulation. If the solitonlike density wave is observed in the simulation, it should be compared with the analytical solution of the traffic model.

In this paper, we carry out the computer simulation for the optimal velocity model with open boundaries. We calculate the fundamental diagram (the traffic current against density). Then, we study the condition such that a density wave appears when a car decelerates instantly. We show that the soliton density wave appears only near the threshold between the jam and no jam and when the strength of deceleration is higher than the threshold, the kink-antikink density wave appears. We give the nonlinear analysis for the optimal velocity model. We obtain the soliton solution of the KdV equation. We compare the analytical solution with the simulation result.

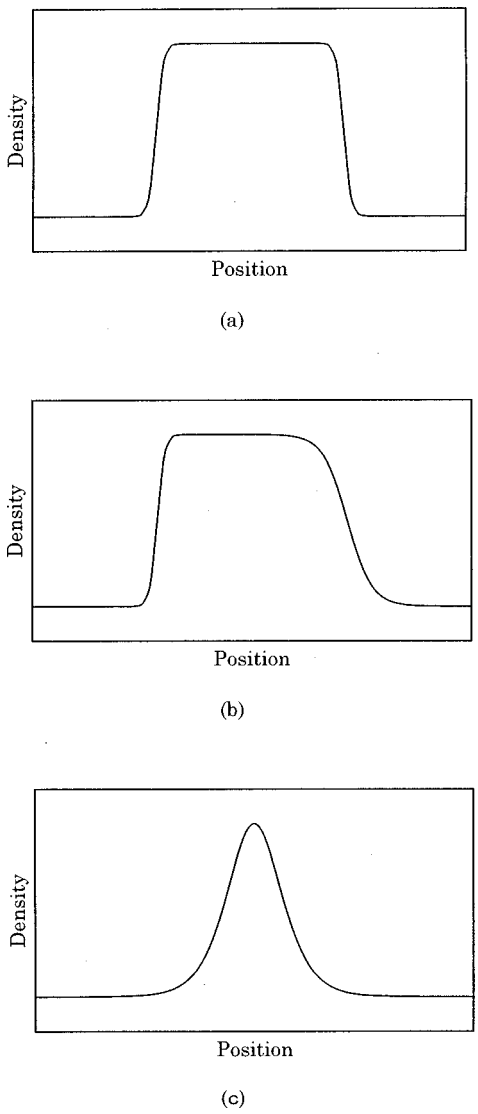

FIG. 1. The schematic profiles of traffic density waves (jams). (a) The symmetric kink-antikink density wave, (b) the asymmetric kink-antikink density wave, and (c) the soliton density wave.

II. SIMULATION AND RESULT

We describe the optimal velocity model proposed by Bando *et al.* [5]. The equation of motion of car n is

$$\frac{d^2x_n}{dt^2}=a\left\{V(\Delta x_n)-\frac{dx_n}{dt}\right\}, \tag{5}$$

where x_n is the position of car n, $\Delta x_n(=x_{n+1}-x_n)$ is the headway of car n, and a is the sensitivity. The inverse of sensitivity a corresponds to the delay time in the other car-following models [28]. $V(\Delta x_n)$ is the optimal velocity. Car n is controlled in such a way that the car velocity adjusts the optimal velocity $V(\Delta x_n)$ depending upon headway. This model is a typical one of the car-following models. This model is known as the optimal velocity model.

The optimal velocity is given by

$$V(\Delta x_n)=\tanh(\Delta x_n-x_c)+\tanh(x_c), \tag{6}$$

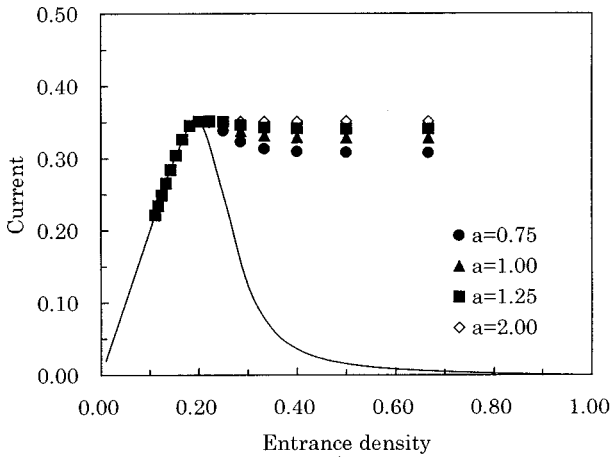

FIG. 2. The plot of the traffic current against the entrance density for sensitivity $a=0.75$, 1.00, 1.25, and 2.00. The circles, triangles, squares, and white diamonds indicate the simulation result. The solid line indicates the analytical result.

where x_c has the order of the safety distance for $v_{\max}$ (the maximal velocity)$=2.0$. The optimal velocity is a function having the following properties: a monotonically increasing function with an upper bound (maximal velocity). The optimal velocity function has a turning point (inflection point) at $\Delta x_n=x_c: V''(x_c)=0$. It is important that the optimal velocity function has a turning point. Otherwise, one cannot derive the modified KdV equation giving traffic jams in terms of a kink density wave.

The above optimal velocity model has been studied by computer simulation only for the periodic boundary condition. It has been shown that the kink density wave (traffic jam) appears below the critical point $a_c=2.0$. We could not find the soliton density wave for the periodic boundary condition. Therefore, we perform computer simulation for the optimal velocity model under the open boundary condition. We consider the one-dimensional road with the entrance and the exit. When a car reaches the exit, its car is removed from the road. Then, the optimal velocity of the front car nearest to the exit becomes the maximal velocity 2.0 since there are no cars in the front of its car. The front car is accelerated by the difference between the maximal and present velocities. If the distance between the entrance and the last car nearest to the entrance comes to be equal to the prescribed value, a new car is introduced at the entrance on the road. The prescribed value is given by $1/\rho_1-1$ where ρ_1 is the car density at the entrance. We define the relationship between the headway and the density as following: $\Delta x=1/\rho-1$. If one adopts $\Delta x=1/\rho$, the density is larger than 1 for $\Delta x<1$ and diverges in the limit $\Delta x\to 0$. Therefore, we adopt the relationship $\Delta x=1/\rho-1$ in order to normalize the density. This relation corresponds to a car length of 1. Equation (5) is calculated numerically by the use of the fourth-order Runge-Kutta method where the time interval is 1/128. Figure 2 shows the plot of the traffic current as a function of the density at the entrance for various values of sensitivity. Here we set $x_c=3.0$. For entrance density lower than 0.2, the current is on the single curve. For larger sensitivity than the critical sensitivity $a_c=2.0$, the current is on the same curve as $a=2.0$. After the current reaches the maximal value, the current is constant for entrance densities higher than 0.2. For sensitiv-

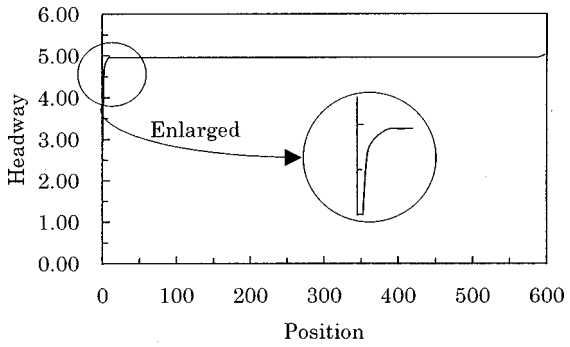

FIG. 3. The density profile obtained at $t=1000$ for sensitivity $a=1.0$ and entrance density $\rho_1=0.5$.

ity lower than 2.0, after the current reaches the maximal value, the current decreases, and becomes a constant value with increasing entrance density. The constant value of current depends on the sensitivity for $a<2.0$ and decreases with sensitivity. It has been shown that the macroscopic models have the same qualitative behavior as the optimal velocity model [31,32]. If no jams appear, the velocity in the steady state is equal to the optimal velocity. In the traffic flow without jams, the current is given by

$$Q=V(\Delta x_n)/(\Delta x_n+1). \tag{7}$$

The current of Eq. (7) is indicated by the solid curve in Fig. 2. For densities lower than 0.2, the current obtained from the simulation agrees with Eq. (7). By differentiating Eq. (7) with headway and taking the derivative to be zero, we find that the maximal current occurs at density 0.2. The density wave does not appear at any density for the open boundaries. On the other hand, the density wave occurs at high density for the periodic boundary when a small disturbance is added to the system.

Figure 3 shows the typical headway profile obtained after $t=1000$ for $a=1.0$ and $\rho_1=0.5$. Except for the neighborhood of the entrance and exit, the headway is a constant and the value equals 5. The headway 5 comes to the density 0.166--, calculated in terms of density. For entrance density larger than 0.2, the density near the center of the road is less than 0.2. In Fig. 4, we plot the traffic current against the

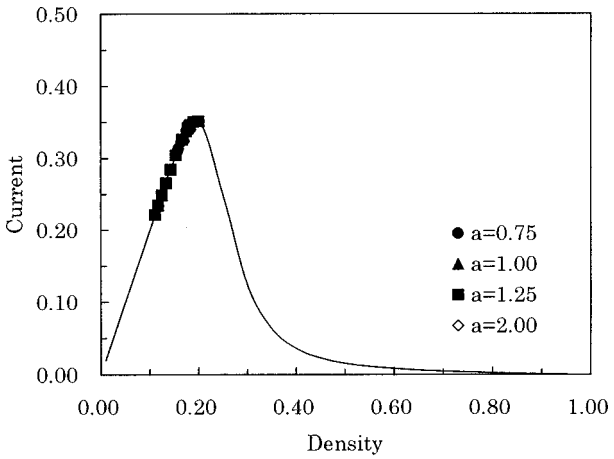

FIG. 4. The plot of the traffic current against the density at the road center for that in Fig. 2.

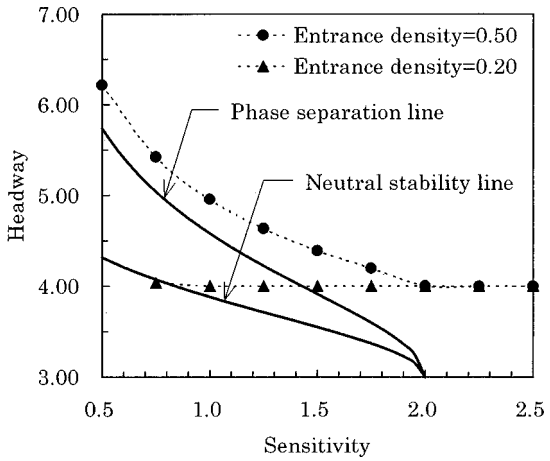

FIG. 5. The plot of the headway at the road center against the sensitivity. The circles and triangles indicate the headways of $\rho_1=0.5$ and $\rho_1=0.2$. The solid lines indicate the phase separation line and the neutral stability line.

density at the road center for that in Fig. 2. The traffic current is on the curve of Eq. (7). Traffic relaxes to free equilibrium traffic regardless of the density at the inflow boundary. We study how headway near the road center changes with the sensitivity for the cases of the entrance densities $\rho_1=0.5$ and $\rho_1=0.2$. Figure 5 shows the plot of the headway at the road center against the sensitivity. The circles and triangles indicate the headways of $\rho_1=0.5$ and $\rho_1=0.2$ for various sensitivities. The phase separation line and the neutral stability line (obtained from the nonlinear analysis and linear stability analysis [5]) are shown by the solid lines. For the high density $\rho_1=0.5$, the headway at the road center increases with decreasing sensitivity. The current is less than the maximal current. The headway is along and above the phase separation line. The density wave (traffic jam) does not occur even if the disturbances are added to this steady state. For $\rho_1=0.2$ yielding the maximal current, the headway at the road center remains the constant 4.0 with decreasing sensitivity until it crosses the neutral stability line. If the disturbances are added to the traffic flow near the crossing point, the density wave (traffic jam) can occur. Except for the neighborhood of the crossing point, the density wave does not occur even if the disturbances are added. The region between the phase separation line and the neutral stability line represents the metastable traffic flow [30]. When the sensitivity is larger than 2.0, the headway at the road center is all the same 4.0. This explains why the traffic current is the maximal current for the sensitivity larger than 2.0 and density higher than 0.2.

We study how the maximal current varies with the safety distance x_c (headway at the turning point of the optimal velocity function). As a result, the headway at maximal current nearly equals the headway at the inflection point $+1$. The simulation result is consistent with the analytical result.

We study whether or not density waves appear when the disturbances are added. We add the disturbances as following: after the traffic flow reaches the steady state, the lead car closest to the exit is decelerated to the prescribed low velocity during ten time steps where the unit time step is one. We call this the slowdown velocity for the prescribed low velocity. For entrance density higher than 0.2, the density wave propagating sufficiently long time does not appear even if the

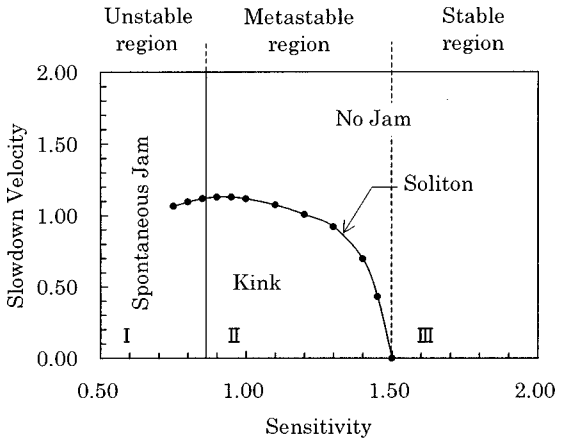

FIG. 6. The region map at headway $\Delta x = 4.0$. The circles indicate the points at which the soliton density wave occurs. The regions I, II, and III represent, respectively, the spontaneous jam, the kink density wave, and no jam.

sensitivity is less than the critical value 2.0. The density wave formed at early stage disappears in time. For the entrance density $\rho_1 = 0.2$ yielding the maximal current, the density wave appears when the sensitivity is between the phase separation line and the neutral stability line and the large disturbance is added. The region map (the plot of the slowdown velocity v_s against the sensitivity) is shown in Fig. 6 where headway Δx is 4.0. The circles indicate the soliton density wave. The regions I, II, and III represent, respectively, the spontaneous jam, the kink density wave, and no jam. The soliton density wave appears only on the boundary

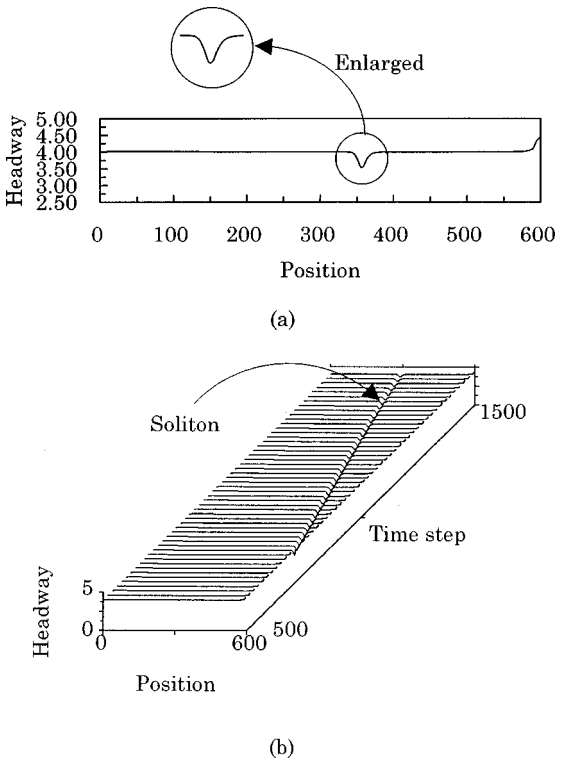

FIG. 7. The density profile (a) at $t = 1300$ and the space-time evolution (b) of headway for $a = 1.0$, $v_s = 1.1175$. The typical soliton density wave is observed.

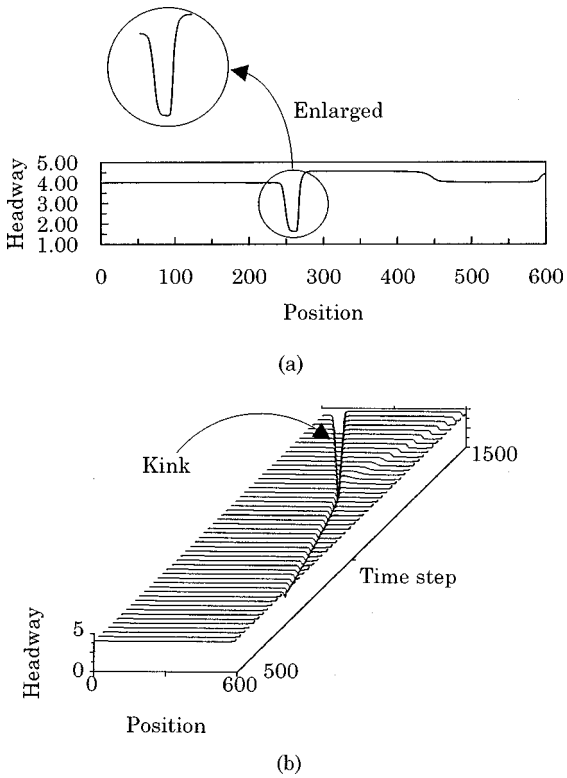

FIG. 8. The density profile (a) at $t = 1300$ and the space-time evolution (b) of headway for $a = 1.0$, $v_s = 1.1170$. The soliton density wave crosses over the kink density wave.

line between the regions II and III. In the region III, the density wave formed at early stage disappears in time. When the sensitivity is between 0.84 and 1.50, the traffic flow is metastable. The soliton density wave is unstable even if perturbations are very small. All perturbations will either develop to the kink-antikink density waves or dissolve in the course of time. It would also mean that real stable localized traffic clusters are never the KdV soliton. As a result, it is concluded that the soliton density wave is observed on the boundary line between the regions of the kink density waves and of the dissolving density waves. When the sensitivity is less than 0.84, the traffic flow is unstable and the kink density wave is formed even if the disturbances are small. The typical space-time evolutions of headway are shown in Figs. 7, 8, and 9. Figure 7 shows the space-time evolution (b) of

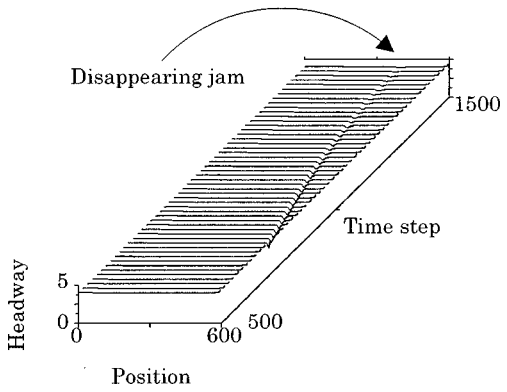

FIG. 9. The space-time evolution of headway for $a = 1.0$, $v_s = 1.1180$. The density wave disappears in time.

headway between $t=500$ and $t=1500$ and the headway profile (a) at $t=1300$ for $a=1.0$, $\nu_s=1.1175$, and $x_c=3.0$. The typical soliton density wave is observed. It propagates backward with the constant velocity. Figure 8 shows the space-time evolution (b) of headway between $t=500$ and $t=1500$ and the headway profile (a) at $t=1300$ for $a=1.0$, $\nu_s=1.1170$, and $x_c=3.0$. The density wave propagates backward. It crosses over the kink density wave from the soliton density wave. The propagation velocity of soliton is less than that of the kink density wave. The width of the kink-antikink pulse increases with time but the height remains a constant. Figure 9 shows the space-time evolution of headway between $t=500$ and $t=1500$ for $a=1.0$, $\nu_s=1.1180$, and $x_c=3.0$. At the early stage, the soliton density wave is formed but disappears in time. Thus, the soliton density wave appears only near the boundary line between the regions II and III.

When a perturbation is added to a uniform traffic flow in the metastable state, both expansion and compression waves occur at the early stage. Then, both waves propagate forward and dissolve in the course of time as the compression wave interferes with the expansion wave. The phenomenon depends little on the location of the perturbation if the location is far from the exit. However, if a perturbation near the exit is added to the metastable traffic flow under the open boundary condition, the expansion wave never appears and only the compression wave propagates backward. In the course of time, the compression wave develops to the kink-antikink density wave.

III. NONLINEAR ANALYSIS

We derive the KdV equation describing the soliton density wave from the optimal velocity model. The linear stability analysis for the optimal velocity model has been done by Bando *et al.* [5]. For later convenience, we carry out the linear stability analysis [5,27]. Equation (5) has the following steady-state solution: $x_n^{(0)}=\Delta x^{(0)}n+V(\Delta x^{(0)})t$ where $\Delta x^{(0)}$ is the constant headway. Let y_n be a small deviation from the uniform steady-state flow: $x_n=x_n^{(0)}+y_n$. Then, the linear equation is obtained from Eq. (5),

$$\frac{d^2y_n}{dt^2}=a\left\{V'(\Delta x^{(0)})\Delta y_n-\frac{dy_n}{dt}\right\}, \tag{8}$$

where $V'(\Delta x^{(0)})=dV(\Delta x)/d\Delta x|_{\Delta x=\Delta x^{(0)}}$. By expanding $y_n\propto\exp(ikn+zt)$, the following equatiion of z is derived:

$$z^2+az-aV'(\Delta x^{(0)})(e^{ik}-1)=0. \tag{9}$$

From Eq. (9), one obtains the neutral stability condition:

$$a_s=2V'(\Delta x^{(0)}). \tag{10}$$

The uniform traffic flow with headway $\Delta x^{(0)}$ and velocity $V(\Delta x^{(0)})$ is stable if the following condition is satisfied:

$$a>2V'(\Delta x^{(0)}). \tag{11}$$

By expanding Eq. (9) with ik near the neutral stability point, one obtains

$$z(k)=\frac{a_s}{2}ik+\frac{a_s-a}{4}k^2-\frac{a_s}{12}ik^3-\frac{a_s}{16}k^4+O(k^5). \tag{12}$$

Suppose the headway of uniform traffic is near the neutral stability point. We quantify this by writing

$$V'(\Delta x^{(0)})-\frac{(a_s-\delta a)}{2}=\frac{\delta a}{2}=\frac{a}{2}\left(\frac{a_s}{a}-1\right),$$

$$\frac{a}{2}\left|\frac{a_s}{a}-1\right|\equiv\beta\varepsilon^2, \tag{13}$$

where ε is an arbitrary parameter and $\beta=a/2$.

We have introduced ε as a small scaling parameter. We consider the slowly varying behavior at long wavelengths near the neutral stability line. We wish to extract slow scales for space variable n and time variable t. We determine the scalings of n and t. The real part of Eq. (12) contains both a fourth-order dissipation term and a negative diffusion term. From the balance of the two terms, k scales as $k\propto\varepsilon$. This leads to the scaling relation $n\propto\varepsilon^{-1}$. The scaling of t is determined by the lowest-order imaginary term in Eq. (12). It is given by a dispersion term of ik^3 since the propagation term of ik is eliminated by shifting to a moving coordinate system. Thus, t scales as $t\propto\varepsilon^{-3}$. For $0<\varepsilon\ll1$, we, therefore, define the slow variables X and T [26–30,33]:

$$X=\varepsilon\cdot(n+bt)\quad\text{and}\quad T=\varepsilon^3t. \tag{14}$$

We rewrite Eq. (5) as follows:

$$\frac{d^2\Delta x_n}{dt^2}+a\frac{d\Delta x_n}{dt}-a[V(\Delta x_{n+1})-V(\Delta x_n)]=0. \tag{15}$$

We expect that an amplitude equation would balance the linear growth term of order ε^4A with a stabilizing nonlinear term of order A^3. Thus, we expect that the disturbance saturates at a size of order ε^2. We, therefore, set the headway as

$$\Delta x_n=\Delta x^{(0)}+\varepsilon^2R(X,T). \tag{16}$$

By inserting Eq. (16) into Eq. (15) and expanding to the sixth order of ε, one obtains the following nonlinear differential equation:

$$\varepsilon^3a(b-V')\frac{\partial R}{\partial X}+\varepsilon^4\left(b^2-\frac{aV'}{2}\right)\frac{\partial^2R}{\partial X^2}+\varepsilon^5a\left[\frac{\partial R}{\partial T}-\frac{V'}{6}\frac{\partial^3R}{\partial X^3}-V''R\frac{\partial R}{\partial X}\right]+\varepsilon^6\left[2b\frac{\partial^2R}{\partial X\partial T}-\frac{aV'}{24}\frac{\partial^4R}{\partial X^4}-\frac{aV''}{4}\frac{\partial^2R^2}{\partial X^2}\right]=0, \tag{17}$$

where $V'=dV/d\Delta x|_{\Delta x=\Delta x^{(0)}}$ and $V''=d^2V/d\Delta x^2|_{\Delta x=\Delta x^{(0)}}$ and we used the expansions shown in the Appendix.

By taking $b=V'$, the third-order term of ε is eliminated. By inserting Eq. (13) into Eq. (17), one obtains

$$\varepsilon^5 a\left[\frac{\partial R}{\partial T}-\frac{V'}{6}\frac{\partial^3 R}{\partial X^3}-V''R\frac{\partial R}{\partial X}\right]+\varepsilon^6\left[\left(\frac{V'^2}{3}-\frac{aV'}{24}\right)\frac{\partial^4 R}{\partial X^4}+\beta V'\frac{\partial^2 R}{\partial X^2}+\left(V'V''-\frac{aV''}{4}\right)\frac{\partial^2 R^2}{\partial X^2}\right]=0, \tag{18}$$

where we used

$$\frac{\partial^2 R}{\partial X\partial T}=\frac{V'}{6}\frac{\partial^4 R}{\partial X^4}+\frac{V''}{2}\frac{\partial^2 R^2}{\partial X^2}+O(\varepsilon).$$

In order to derive the regularized equation, we make the following transformations:

$$T=\sqrt{(V'/6|g|^3)}T',\quad X=-\sqrt{(V'/6|g|)}X',$$

$$\text{and } R=\frac{|g|}{V''}R', \tag{19}$$

where g is a negative constant. With the use of Eq. (19), one obtains the regularized equation,

$$\varepsilon^5 a\frac{g^2}{V''}\sqrt{(6|g|/V')}\left[\frac{\partial R'}{\partial T'}+\frac{\partial^3 R'}{\partial X'^3}+R'\frac{\partial R'}{\partial X'}\right]+\varepsilon^6\frac{6g^2}{V'V''}\left[\beta V'\frac{\partial^2 R'}{\partial X'^2}+2|g|\left(V'-\frac{a}{8}\right)\frac{\partial^4 R'}{\partial X'^4}+|g|\left(V'-\frac{a}{4}\right)\frac{\partial^2 R'^2}{\partial X'^2}\right]=0. \tag{20}$$

If one ignores the $O(\varepsilon^6)$ terms in Eq. (20), it is just the KdV equation with a soliton solution as the desired solution,

$$R_0'(X',T')=A\,\mathrm{sech}^2\left[\sqrt{(A/12)}\left(X'-\frac{A}{3}T'\right)\right]. \tag{21}$$

Amplitude A of soliton solutions of the KdV equation is a free parameter. The perturbation terms $O(\varepsilon^6)$ of perturbed KdV equation (20) select a unique member of the continuous family of KdV solitons.

Next, assuming that $R'(X',T')=R_0'(X',T')+\varepsilon R_1'(X',T')$, we take into account the $O(\varepsilon)$ correction. In order to determine the selected value of A for the soliton solution (21), it is necessary to satisfy the solvability condition,

$$(R_0',M[R_0'])\equiv\int_{-\infty}^{\infty}dX'R_0'M[R_0']=0, \tag{22}$$

where $M[R_0']$ is the $O(\varepsilon^6)$ term of Eq. (20).

By performing the integration, one obtains the selected value

$$A=\frac{14V'}{3|g|}. \tag{23}$$

By rewriting each variable to the original one, one obtains the soliton solution of the headway:

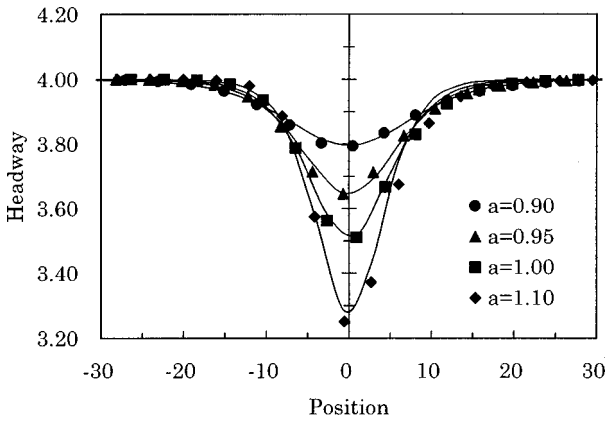

FIG. 10. The plot of the headway against the position within the soliton density wave. The circle, triangle, square, and diamond points indicate, respectively, the simulation result for $a=0.90$, 0.95, 1.00, and 1.10. The analytical results are represented by the solid curves.

$$\Delta x_n=\Delta x^{(0)}+\frac{14V'}{3V''}\left|\frac{a_s}{a}-1\right|\mathrm{sech}^2\times\left[\sqrt{(7|a_s/a-1|/3)}\left\{n+\left(1+\frac{14\left|\frac{a_s}{a}-1\right|}{9}\right)V't\right\}\right]. \tag{24}$$

We show the analytical result in Fig. 10. The solid curves indicate, respectively, the plots of the headway against the position for sensitivity $a=0.90$, 0.95, 1.00, and 1.10. The circle, triangle, square, and diamond points indicate, respectively, the simulation result for $a=0.90$, 0.95, 1.00, and 1.10. The analytical results are in good agreement with the simulation results near the neutral stability point. Figure 11 shows the plot of the propagation velocity of soliton against sensitivity. The solid curve indicates the analytical result. The circles indicate the simulation result. The simulation result agrees with the analytical result near the neutral stability point.

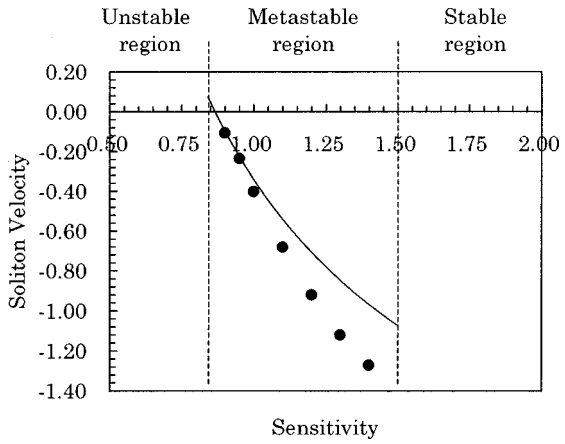

FIG. 11. The plot of the propagation velocity of soliton against sensitivity. The solid curve represents the analytical result. The circles indicate the simulation result.

For comparison, we shortly describe the derivation of the modified KdV equation of the kink density wave. The derivative V' of the optimal velocity has the maximal value at the turning point $\Delta x_n = \Delta x_c$. Therefore, in Eq. (10), there exists a critical value of a, denoted by a_c. Above the critical point, the jamming transition never occurs irrespectively of density. From the parabolic form of the neutral stability line near the critical point, it is expected that the amplitude of the density wave scales as $A \propto \varepsilon$ [27]. We set the headway as

$$\Delta x_n = \Delta x_c + \varepsilon R(X,T). \tag{25}$$

We note that the kink density wave is obtained by expanding the headway ''around the critical point'' and the soliton density wave is derived by expanding the headway ''near the neutral stability line.'' By inserting Eq. (25) into Eq. (15) and expanding to the fifth order of ε, one obtains the modified KdV equation with the perturbed term. Finally, one obtains the kink solution of the headway:

$$\Delta x_n = \Delta x_c \pm \sqrt{(5V'(\Delta x_c)|a_c/a-1|/|V'''(\Delta x_c)|)} \times \tanh\left[\sqrt{(5|a_c/a-1|/2)} \times \left\{ n + \left(1 - \frac{5}{6}\left|\frac{a_c}{a}-1\right|\right) V'(\Delta x_c)t \right\}\right], \tag{26}$$

where a_c is the value 2.0 of sensitivity at the critical point and $V'(\Delta x_c)$ is the derivative of optimal velocity function at the critical point. The modified KdV equation is derived near the critical point $(a_c, \Delta x_c)$ [27]. However, the kink density wave solutions agree with the simulation result far from the critical point [27–30]. The kink-antikink density wave observed in our simulation of Sec. II looks similar to the modified KdV solution. On the other hand, the KdV equation describing the soliton is derived only near the neutral stability line. The KdV equation has been derived from the hydrodynamic model by Kurtze and Hong [26]. However, they have not been compared with the simulation result. They have concluded that the asymmetric kink-antikink density wave found by Kerner and Konhauser [22] is described by the soliton density wave.

We note that we did not find the soliton density wave in the simulation with a periodic boundary condition. This is due to the interfering of the compressive wave with the expanding wave when a disturbance is added to the uniform flow for the periodic system. We could find the soliton density wave for the open boundary system.

IV. SUMMARY

We have investigated the traffic flow for the open boundary condition. We have found that the traffic current saturates at the maximal current and no jam appears without disturbances. We have shown that when the slowing down larger than the threshold occurs, the two types of traffic jams appear: one is the soliton density wave appearing on the threshold and the other is the kink density wave. We have analyzed the optimal velocity model and derived the KdV equation near the neutral stability line. We have obtained the soliton solution analytically. We have shown that the simulation result is consistent with the analytical result of the soliton density wave.

To our knowledge, until now, the soliton density wave has not been distinguished with the kink density wave. In the literature of traffic, the kink density wave has been confused with the soliton density wave. We have clarified the difference between the soliton and kink density waves.

APPENDIX

In this appendix, we give the expansions of each terms in Eq. (15) to sixth order of ε.

$$\frac{d\Delta x_n}{dt} = \varepsilon^3 b \frac{\partial R}{\partial X} + \varepsilon^5 \frac{\partial R}{\partial T}, \tag{A1}$$

$$\frac{d^2\Delta x_n}{dt^2} = \varepsilon^4 b^2 \frac{\partial^2 R}{\partial X^2} + 2\varepsilon^6 b \frac{\partial^2 R}{\partial X \partial T}, \tag{A2}$$

$$\Delta x_{n+1} = \Delta x^{(0)} + \varepsilon^2 R + \varepsilon^3 \frac{\partial R}{\partial X} + \varepsilon^4 \frac{1}{2}\frac{\partial^2 R}{\partial X^2} + \varepsilon^5 \frac{1}{6}\frac{\partial^3 R}{\partial X^3} + \varepsilon^6 \frac{1}{24}\frac{\partial^4 R}{\partial X^4}, \tag{A3}$$

$$V(\Delta x_{n+1}) - V(\Delta x_n) = \varepsilon^3 V' \frac{\partial R}{\partial X} + \varepsilon^4 \frac{1}{2} V' \frac{\partial^2 R}{\partial X^2} + \varepsilon^5 \left[\frac{V'}{6}\frac{\partial^3 R}{\partial X^3} + V'' R \frac{\partial R}{\partial X}\right] + \varepsilon^6 \left[\frac{V'}{24}\frac{\partial^4 R}{\partial X^4} + \frac{V''}{4}\frac{\partial^2 R^2}{\partial X^2}\right]. \tag{A4}$$

By inserting Eqs. (A1)–(A4) into Eq. (15), one obtains Eq. (17).

[1] *Traffic and Granular Flow*, edited by D. E. Wolf, M. Schreckenberg, and A. Bachem (World Scientific, Singapore, 1996).
[2] D. Helbing, *Verkehrsdynamik* (Springer, Berlin, 1997).
[3] G. F. Newell, Oper. Res. **9**, 209 (1961).
[4] G. B. Whitham, Proc. R. Soc. London, Ser. A **428**, 49 (1990).
[5] M. Bando, K. Hasebe, A. Nakayama, A. Shibata, and Y. Sugiyama, Phys. Rev. E **51**, 1035 (1995).
[6] K. Nagel and M. Schreckenberg, J. Phys. I **2**, 2221 (1992).

[7] M. Schreckenberg, A. Schadschneider, K. Nagel, and N. Ito, Phys. Rev. E **51**, 2329 (1995).
[8] G. Csanyi and J. Kertestz, J. Phys. A **28**, 427 (1995).
[9] S. C. Benjamin, N. F. Johnson, and P. M. Hui, J. Phys. A **29**, 3119 (1996).
[10] A. Schadschneider and M. Schreckenberg, Ann. Phys. (N.Y.) **6**, 541 (1997).
[11] O. Biham, A. A. Middelton, and D. A. Levine, Phys. Rev. A **46**, R6124 (1992).
[12] T. Nagatani, Phys. Rev. E **48**, 3290 (1993).
[13] J. A. Cuesta, F. C. Matinez, J. M. Nolera, and A. Sanchez, Phys. Rev. E **48**, 4175 (1993).
[14] K. H. Chung, P. M. Hui, and G. Q. Gu, Phys. Rev. E **51**, 772 (1995).
[15] E. Ben-Naim, P. L. Krapivsky, and S. Redner, Phys. Rev. E **50**, 822 (1994).
[16] T. Nagatani, Phys. Rev. E **51**, 922 (1995).
[17] I. Prigogine and R. Herman, *Kinetic Theory of Vehicular Traffic* (Elsevier, New York, 1971).
[18] S. L. Paveri-Fontana, Transp. Res. **9**, 225 (1975).
[19] D. Helbing, Phys. Rev. E **53**, 2366 (1996).
[20] D. Helbing, Physica A **233**, 253 (1996).
[21] T. Nagatani, Physica A **237**, 67 (1997).
[22] B. S. Kerner and P. Konhauser, Phys. Rev. E **48**, 2335 (1993).
[23] B. S. Kerner, P. Konhauser, and M. Schilke, Phys. Rev. E **51**, 6243 (1995).
[24] S. Krauss, P. Wagner, and C. Gawron, Phys. Rev. E **55**, 5597 (1997).
[25] B. S. Kerner and H. Rehborn, Phys. Rev. E **53**, R1297 (1996).
[26] D. A. Kurtze and D. C. Hong, Phys. Rev. E **52**, 218 (1995).
[27] T. Komatsu and S. Sasa, Phys. Rev. E **52**, 5574 (1995).
[28] T. Nagatani, K. Nakanishi, and H. Emmerich, J. Phys. A **31**, 5431 (1998).
[29] T. Nagatani and K. Nakanishi, Phys. Rev. E **57**, 6415 (1998).
[30] T. Nagatani, Phys. Rev. E **58**, 4271 (1998).
[31] M. Treiber, A. Hennecke, and D. Helbing, Phys. Rev. E **59**, 239 (1999).
[32] M. Hermann and B. S. Kerner, Physica A **250**, 163 (1998).
[33] M. C. Cross and P. C. Hohenberg, Rev. Mod. Phys. **65**, 851 (1993).